JOURNAL OF MATERIALS SCIENCE **41** (2006) 147–153

Fredholm integral equation of the Laser Intensity Modulation Method (LIMM): Solution with the polynomial regularization and L-curve methods

SIDNEY B. LANG
Department of Chemical Engineering, Ben-Gurion University of the Negev, 84105 Beer Sheva, Israel
E-mail: lang@bgu.ac.il

The Laser Intensity Modulation Method (LIMM) is widely used for the determination of the spatial distribution of polarization in polar ceramics and polymers, and space charge in non-polar polymers. The analysis of experimental data requires a solution of a Fredholm integral equation of the 1st kind. This is an ill-posed problem that has multiple and very different solutions. One of the more frequently used methods of solution is based upon Tikhonov regularization. A new method, the Polynomial Regularization Method (PRM), was developed for solving the LIMM equation with an 8th degree polynomial using smoothing to achieve a stable and optimal solution. An algorithm based upon the L-curve method (LCM) was used for the prediction of the best regularization parameter. LIMM data were simulated for an arbitrary polarization distribution and were analyzed using PRM and LCM. The calculated distribution function was in good agreement with the simulated polarization distribution. Experimental polarization distributions in a poorly poled sample of polyvinylidene fluoride (PVDF) and in a $LiNbO_3$ bimorph, and space charge in polyethylene were analyzed. The new techniques were applied to the analysis of 3-dimensional polarization distributions.

1. Introduction

1.1. LIMM experiment

LIMM was first suggested by Lang and Das-Gupta in 1981 [1] and described in detail in 1986 [2]. A review of the current implementation was presented in 2004 [3]. The experimental technique is as follows. LIMM samples are prepared as thin plates or sheets with their flat surfaces normal to the polar axis. These surfaces are coated with very thin opaque electrodes. The sample may be either freely suspended or attached to a grounded metal plate by an electrically conductive paste or cement. The surface of the sample is exposed to a laser beam whose intensity is modulated sinusoidally by means of an acoustooptic modulator or a built-in modulator in the laser. The energy of the laser beam is absorbed at the electrode and heat diffuses into the sample as temperature waves. The depth of penetration of the waves is greater for low modulation frequencies and less for high ones. This produces a spatially non-uniform time-varying temperature distribution that interacts with the unknown polarization or space charge distribution to produce a pyroelectric current. The real and the imaginary components of the current generated at each of 50 to 100 different frequencies are amplified and a lock-in amplifier is used to determine the amplitude and phase relative to that of the modulated intensity of the laser beam.

1.2. Analysis of LIMM data

The relative polarization distribution, $\beta(z)$, is found from a solution of the LIMM equation [2, 4, 5]:

$$I(\omega) = \frac{A}{L}\int_{z_1}^{z_2} \beta(z)\frac{\partial T(z,\omega)}{\partial t}dz \qquad (1)$$

where

$$\beta(z) = \alpha_P P(z) - (\alpha_x - \alpha_\varepsilon)\varepsilon\varepsilon_0 E(z)$$

0022-2461
DOI: 10.1007/s10853-005-5983-8

TABLE I Nomenclature

Parameter	Symbol	Units
A	Laser beam cross-section	m^2
I	Current	A
E	Electric field	Vm^{-1}
k	Thermal conductivity	$Wm^{-1}\ K^{-1}$
L	Thickness	m
p	Pyroelectric coefficient	$Cm^{-2}\ K^{-1}$
P	Polarization	Cm^{-2}
P_S	Spontaneous polarization	Cm^{-2}
r	Regularization parameter	Dimensionless
T	Temperature	K
t	Time	s
z	Spatial coordinate	m
z_1, z_2	Spatial coordinates of upper (irradiated) and lower surfaces of sample	m
α	Thermal diffusivity	$m^2\ s^{-1}$
α_P	Temperature dependence of polarization	K^{-1}
α_x	Thermal expansion coefficient	K^{-1}
α_ε	Temperature dependence of permittivity	K^{-1}
$\beta(z)$	Polarization distribution function (Equation 1)	$Cm^{-2}\ K^{-1}$
γ	Scale factor in Equation 2	Dimensionless
ε	Relative permittivity	Dimensionless
ε_0	Permittivity of vacuum	Fm^{-1}
η	Roughness residual in Equation 6	$C^2\ m^{-7}\ K^{-2}$
λ	Coefficient in Equation 2	Dimensionless
ρ	Data fit residual in Equation 5	A^2
σ	Space charge	Cm^{-3}
ω	Radial frequency	$rad\ s^{-1}$

Nomenclature is given in Table I. The term $\partial T/\partial t$ is calculated from the one-dimensional heat conduction equation using boundary conditions appropriate for either a freely-suspended sample or a sample mounted on a substrate [3]. It was shown by a finite-element solution that the use of a one-dimensional analysis instead of the true three-dimensional one introduces negligible error. Equation 1 is then solved for $\beta(z)$ using experimental measurements of $I(\omega)$. If the experimental sample is a polar ceramic or polymer, it is assumed that the polarization is locally compensated by space charge and only $P(z)$ is determined. If the sample is nonpolar, then $P(z) = 0$ and the electric field $E(z)$ is found. From this, the space charge distribution can be determined. There is no way to separate polarization and space charge if both are present. It should be noted that $I(\omega)$ contains experimental errors. Computer roundoff will effectively add errors, even in the case of computer simulated data. Equation 1 is a Fredholm integral equation of the first kind and is an ill-conditioned problem with a large (possibly infinite) number of very different solutions. An illustration of the multiplicity of solutions was given by Phillips [6]. A term such as $sin(kz)$ can be added to $\beta(z)$. Provided that k is sufficiently large, the integration will reduce this added factor to less than the experimental errors.

A large number of methods have been proposed for the solution of Equation 1 [3]. The most successful of the methods are various forms of the regularization method [7–11] and the scale transformation [4, 5]. The regularization method utilizes the requirement that the polarization distribution must be smooth. By specifying the degree of smoothing, extreme minima and/or maxima are excluded but moderate ones are permitted. However, its usage requires complex computer programs. The scale transformation method is very easy to implement. It is less accurate than regularization and it does not allow the determination of the polarization in regions closer to the sample electrode than the thermal diffusion length at the highest measured frequency. Recently, Lang [3] proposed a simplified regularization method called the Polynomial Regularization Method (PRM). It is implemented using the computer software program, *Mathematica*® [12]. Analysis of experimental data requires the selection of an appropriate regularization parameter. A technique called the L-curve Method (LCM) is used for that purpose. PRM and LCM are described in the following section.

2. Polynomial regularization method (PRM) and L-curve Method (LCM)

2.1. Polynomial regularization method and simulated data

PRM is implemented by assuming that $\beta(z)$ can be represented by an eighth-degree polynomial:

$$\beta(z) = \lambda_0 + \lambda_1\gamma(z) + \lambda_2\gamma(z)^2 + \lambda_3\gamma(z)^3 + \cdots \tag{2}$$

where

$$\gamma(z) = \frac{Log(z) - Log(z_1)}{Log(z_2) - Log(z_1)}$$

Because LIMM is most useful in determining distributions near the sample surface [13], the distribution is based on a normalized logarithmic scale. Polynomials of degrees greater than eight have been found to give very inaccurate results. Lower degree polynomials gave the general shape of the distributions but did not correspond to them in detail. Eighth-degree polynomials were the most satisfactory. The coefficients λ_j, must be determined. Equation 2 is substituted into Equation 1 and the integral is evaluated numerically to give the real and imaginary parts of $I(\omega)_{calc}$ as a function of the λs. A linear regression (least-squares) solution can be obtained by minimizing the function:

$$\sum_i [I(\omega_i)_{exp} - I(\omega_i)_{calc}]^2 \tag{3}$$

with respect to the λs which are then inserted into Equation 2. This yields one possible polarization distribution

but, most likely, an incorrect one. In the regularization technique, the following function is minimized with respect to the λs:

$$\sum_i [I(\omega_i)_{\text{exp}} - I(\omega_i)_{\text{calc}}]^2 + r^2 \int_{z_1}^{z_2} \left(\frac{d^2\beta(z)}{dz^2} \right)^2 dz \quad (4)$$

The regularization parameter, r, smoothes the computed polarization distribution. If $r = 0$, the conventional linear regression solution is found. This solution will have a number of large maxima and minima because of the ill-posed nature of the problem. If r is too large, all of the detail is removed from the computed distribution.

Simulated experimental data will be used to illustrate the PRM. The sample is assumed to be a 25.4-μm thick film of polyvinylidene fluoride (PVDF) with 100-nm thick aluminum electrodes. The lower surface of the sample is in good thermal contact with a thick metallic substrate. A typical frequency range over which data are measured extends from 10 Hz to 100 kHz. Based on the Frequency Range Function proposed by Lang [3], the polarization can be found in the region between 0.01 μm and 10 μm from the laser-irradiated electrode. A polarization distribution, $P(z)$, is assumed, as shown in Fig. 1. This distribution is a purely arbitrary function and does *not* resemble a physically realistic distribution. Then simulated experimental data, $I(\omega)_{\text{exp}}$, are calculated by substituting the distribution into Equation 1. In order that the simulated data will more closely resemble true data, a Gaussian distribution of error is added to each point (standard deviation of 5% of the range of the real and imaginary parts, resp.). The resulting simulated real and imaginary values of current $I(\omega)_{\text{exp}}$ as functions of frequency are shown in Fig. 2. Because the simulated distribution is known, it is possible to examine the closeness of the solution to the true value by varying r. In Fig. 3, the sum of the squares of the differences between $I(\omega)_{\text{exp}}$ and $I(\omega)_{\text{calc}}$ (error of fit) is graphed as a function of r. The minimum error of fit is found for $r = 0.000033$, referred to as the "optimal" value. Calculated distributions for $r = 0$, a very large value of r (0.001) and the optimal value of r (0.000033) are shown in Fig. 4. All three calculated distributions are correct mathematical solutions of Equation 1 but only the distribution corresponding to the optimal value of r reproduces the true distribution.

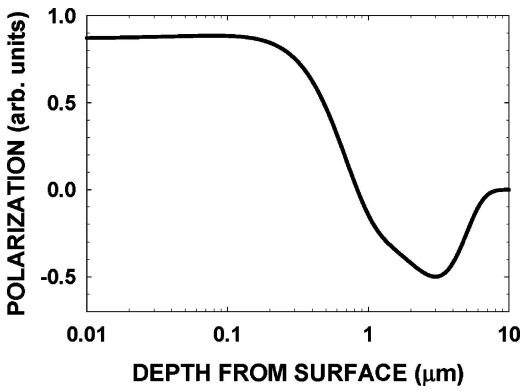

Figure 1 Simulated polarization distribution in 25.4-μm thick PVDF.

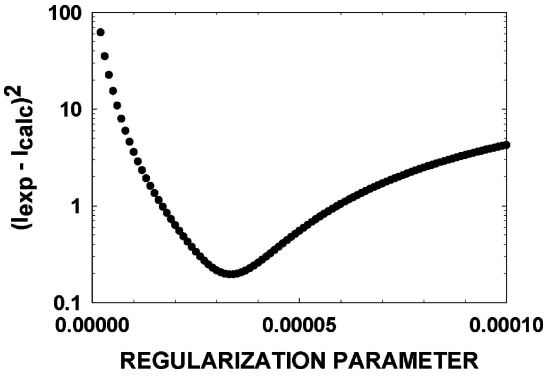

Figure 3 Error of fit versus regularization parameter. Error of fit is sum of squares of differences between true distribution (Fig. 1) and calculated distribution.

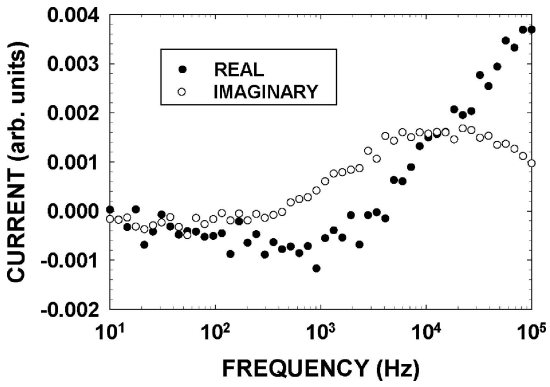

Figure 2 LIMM current versus frequency data calculated from data in Fig. 1 using Equation (1). Random errors added.

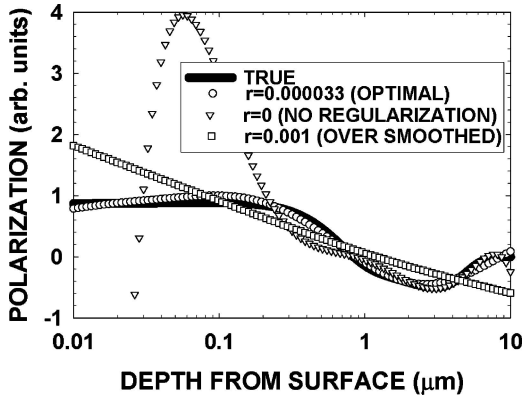

Figure 4 Polarization distributions. True value and those corresponding to no regularization, optimal regularization and oversmoothing.

2.2. L-curve method (LCM) and experimental data

If measured experimental data are analyzed, the optimal value of r cannot be found as illustrated above because the true polarization distribution is unknown. Therefore, a method of selecting a good value of the regularization parameter is required. Several techniques for determination of the regularization parameter are described by Sandner *et al.* [11]. Mellinger [14] has presented an example of the unbiased iterative method. Hansen and O'Leary [15] suggested using the L-curve method for other types of ill-conditioned problems. A range of values of r is selected and two parameters are computed for each value of r. One is the data fit residual:

$$\rho(r) = \sum_{\omega_i} [I(\omega_i)_{\text{exp}} - I(\omega_i)_{\text{calc}}]^2 \tag{5}$$

and the second is the roughness residual:

$$\eta(r) = \int_{z_1}^{z_2} \left(\frac{d^2\beta(z)}{dz^2} \right)^2 dz \tag{6}$$

The data fit residual is a function of the difference between the actual experimental data and values computed for a specific level of r. The roughness residual is a measure of the lack of smoothness in the computed polarization distributions. If $\log(\rho)$ is plotted versus $\log(\eta)$, a curve with an L-shape results. The L-curve for the data in the example above is shown in Fig. 5. The corner corresponds to the point where the calculated distribution $\beta(z)$ changes from domination by large differences between experimental and calculated values to domination by over smoothing. The value of r corresponding to the corner is a good measure of the regularization parameter. It can be found most easily by finding the maximum of the curvature of the function in Fig. 5. The curvature is given by

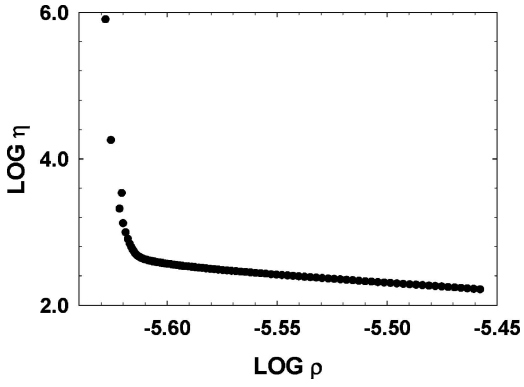

Figure 5 L-curve for simulated data.

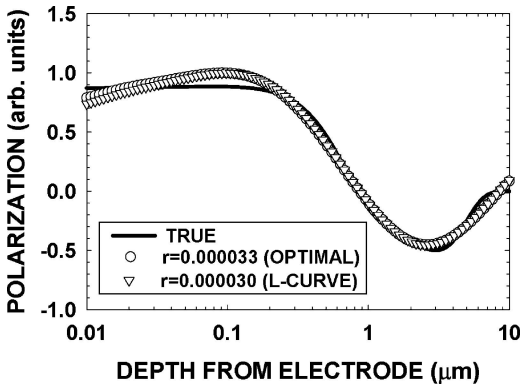

Figure 6 Polarization distributions. True and those corresponding to optimal and L-curve regularization parameters.

the following formula [15]

$$\frac{\hat{\rho}'\hat{\eta}'' - \hat{\rho}''\hat{\eta}'}{\left[(\hat{\rho}')^2 + (\hat{\eta}')^2\right]^{3/2}} \tag{7}$$

where

$$\hat{\rho} = \log(\rho) \quad \text{and} \quad \hat{\eta} = \log(\eta)$$

The $'$ and $''$ symbols indicate differentiation and double differentiation with respect to r. In order to evaluate Equation 7, the values of $\rho(r)$ and $\eta(r)$ are interpolated with low-order polynomials and then differentiated with respect to r. The maximum value of curvature in this example corresponds to $r = 0.000030$. Fig. 6 shows the true polarization distribution, the one corresponding to the optimal value of r and the one found using the L-curve. The "optimal" and the "L-curve" fits are both in excellent agreement with the true curve.

3. Experimental studies

Experimental studies on three different materials are presented here.

3.1. Polyvinylidene fluoride

LIMM data were measured on a 25.4-μm thick sample of polyvinylidene fluoride (PVDF). The sample had been weakly poled and then stored for a number of years. The experimental data are shown in Fig. 7. The regularization parameter at the point of maximum curvature in the L-curve plot (Fig. 8) was 0.000235. Although it is difficult to determine the point of maximum curvature by eye, it is easily found by use of Equation 7. The calculated polarization distribution shown in Fig. 9 is very non-uniform as a consequence of the poling and aging conditions.

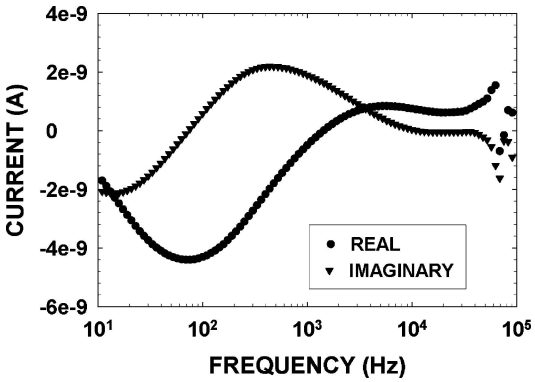

Figure 7 Real and imaginary LIMM data for a poorly-poled sample of PVDF.

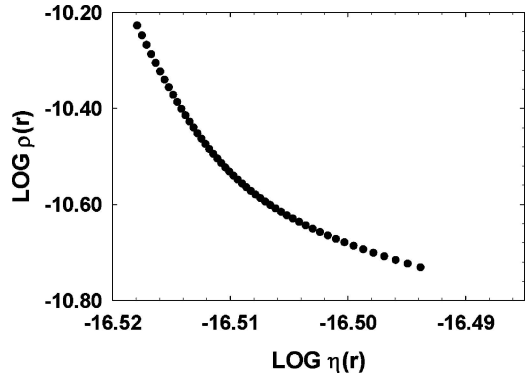

Figure 8 L-curve for PVDF data.

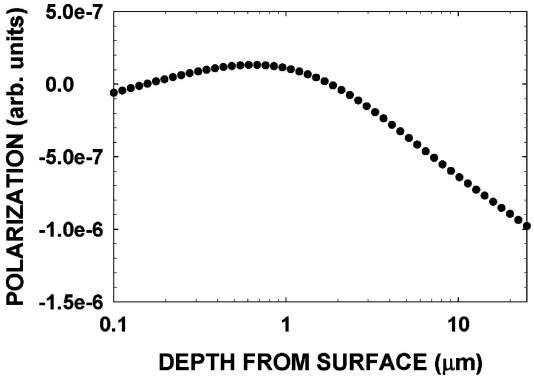

Figure 9 Polarization distribution of PVDF.

3.2. Domain inversion in lithium niobate

Periodic domain inversion has been used to produce wave guides for second harmonic generation in lithium niobate and lithium tantalate [16]. A 0.503-mm thick z-cut plate of $LiNbO_3$ was thermally treated in order to partially invert the orientation of the domains [17]. Domain inversion occurred at the +c-surface and extended approximately halfway through the thickness of the sample. LIMM data were measured in order to determine the resulting polarization distribution [18]. The experimental data for the +c and −c surfaces are shown in Fig. 10. The regular-

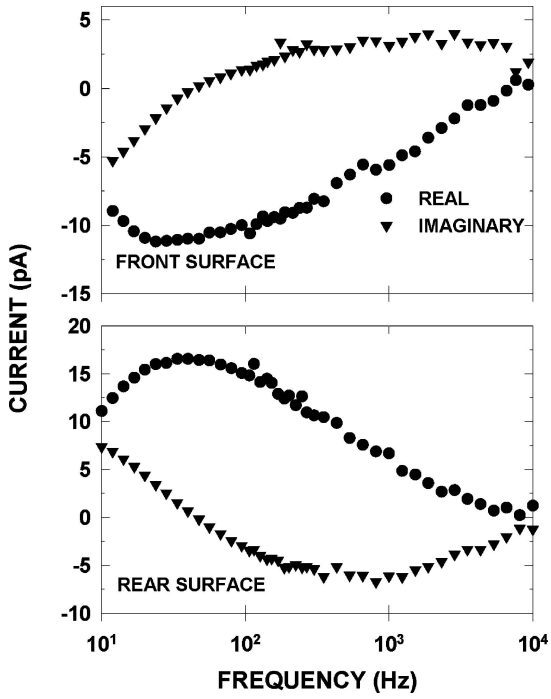

Figure 10 LIMM data for bimorph sample of $LiNbO_3$. Data measured for laser impingement on front and rear surfaces.

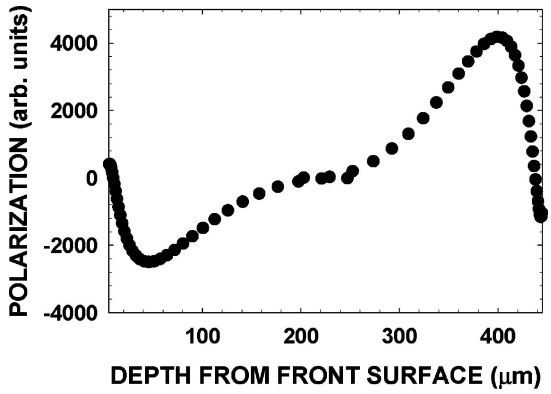

Figure 11 Polarization distribution of bimorph sample of $LiNbO_3$.

ization parameters at the points of maximum curvature in the two L-curve plots were 0.0000591 and 0.0000485, respectively. The domain inversion is clearly shown by the calculated polarization distribution (Fig. 11).

3.3. Space charge in cross-linked polyethylene

Samples of 100-μm thick cross-linked polyethylene (XLPE) were poled with a dc electric field of 50 kV mm^{-1} at room temperature for a period of 18 h [19]. XLPE is non-polar although the presence of polar impurities resulted in some polarization which decayed very rapidly. However, the major effect was the deposition of space

charge. The LIMM data for measurements on the upper and lower surfaces of the sample are shown in Figs 12 and 13. The thermal expansion coefficient α_x used in the calculations was 200×10^{-6} K^{-1} and α_ε was assumed to equal zero. The corresponding regularization parameter was 0.0000235 for each of the surfaces. The electric field distribution in the sample is shown in Fig. 14. The space charge distribution was calculated from the electric field

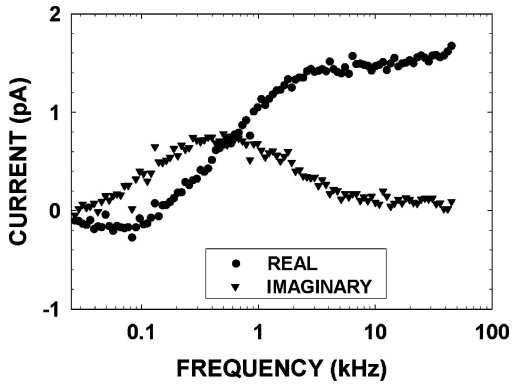

Figure 12 LIMM data for laser impingement on upper surface of cross-linked polyethylene.

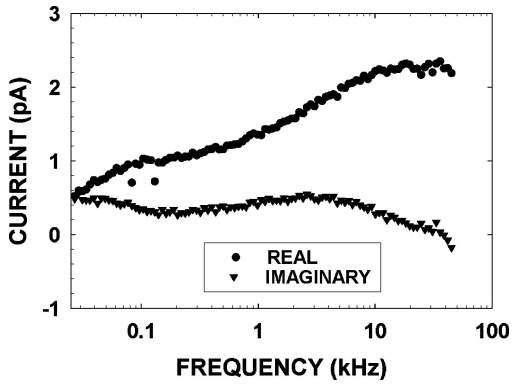

Figure 13 LIMM data for laser impingement on lower surface of cross-linked polyethylene.

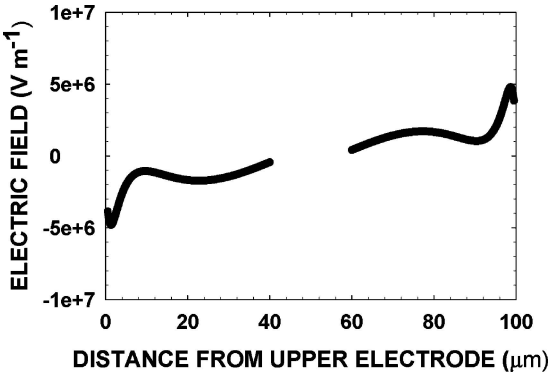

Figure 14 Electric field distribution in cross-linked polyethylene.

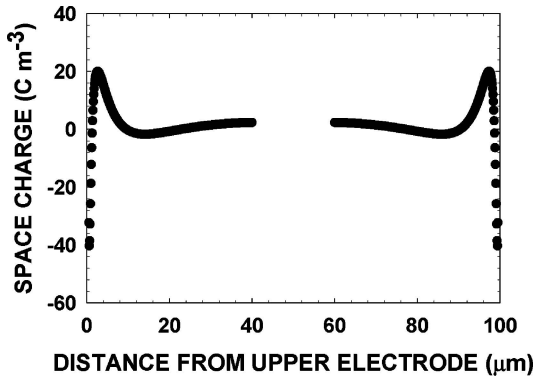

Figure 15 Space charge distribution in cross-linked polyethylene.

distribution by use of Gauss's law:

$$\sigma(z) = \varepsilon_0 \varepsilon \frac{dE}{dz} \tag{8}$$

where $\varepsilon = 2.3$. The space charge distribution is shown in Fig. 15. Negative space charge was found in regions very close to the electrodes. Because of its limited resolution near sample surfaces, the scale transformation technique for analyzing LIMM data [4] did not reveal this negative charge.

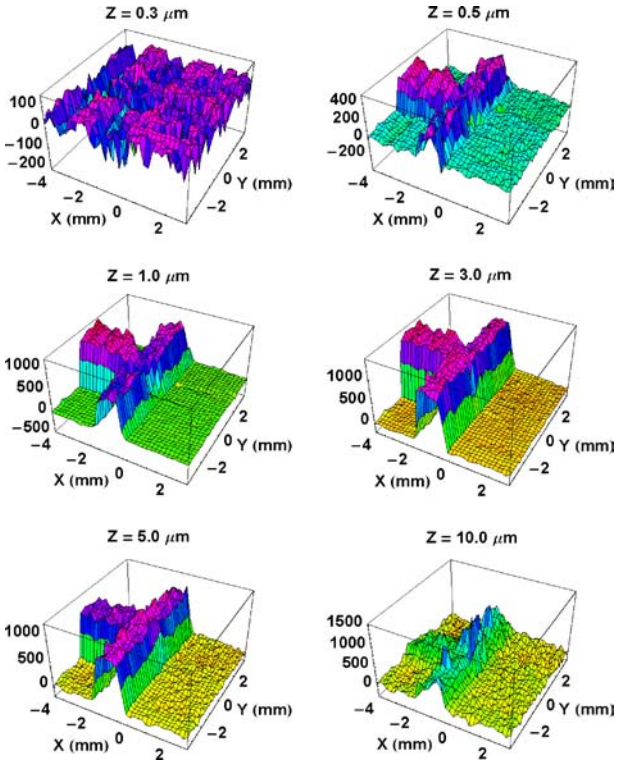

Figure 16 Polarization distributions at various depths in PVDF poled with a T-shaped electrode.

4. Three-dimensional mapping of polarization profiles

The techniques of PRM and LCM were applied to the analysis of three-dimensional polarization data [20]. An 11-μm thick sample of electroded PVDF was affixed to a metallic substrate. It was poled with a dc electric field of 100 MVm^{-1} using a T-shaped electrode. A thermal pulse method of data acquisition rather than LIMM was used. The second-harmonic beam of a Q-switched Nd:YAG laser was focused to a spot size with a radius of 200 μm (at the 1/e point) and was scanned over the sample in a 36 by 36 point-raster pattern. The pulse duration was about 5 ns and 30 to 50 pulses were averaged at each point of the scan. The scan points were 200 μm apart covering a 7$\times$7-mm area. A current amplifier was used and the current versus time data were recorded with a digital storage oscilloscope. The recorded data were Fourier-transformed to yield current versus frequency data. This resulted in conventional LIMM data with a frequency range from 50 Hz to 1 MHz. Thr PRM-LCM analysis was carried out on the 1296 data points. Fig. 16 shows the polarization distributions at various depths from the upper surface of the PVDF. The results were noisy at the shallowest depth of 0.3 μm but very clearly showed the T-shaped distribution at greater depths. At a depth of 10 μm, the polarization began to fade into the background. Future studies will use a more strongly focused laser beam.

5. Conclusions

A new method for the solution of the Fredholm integral equation of LIMM is proposed. It utilizes a regularization approach to find an 8th degree polynomial approximation to the polarization distribution. The value of the regularization parameter is found using the L-curve method. Both simulated and experimental LIMM data were analyzed. Very good agreement was found between the calculated and the true distribution of the simulated data. The experimental measurements revealed useful information concerning polarization or space charge. The technique has now been extended to the analysis of three-dimensional data. The calculations were implemented using *Mathematica* [12]. Copies of the computer files developed in this study are available from the author.

References

1. S. B. LANG and D. K. DAS-GUPTA, *Ferroelectrics* **39** (1981) 1249.
2. *Idem., J. Appl. Phys.* **59** (1986) 2151.
3. S. B. LANG, *IEEE Trans. Dielectr. Electr. Insul.* **11** (2004) 3.
4. B. PLOSS, R. EMMERICH and S. BAUER, *J. Appl. Phys.* **72** (1992) 5363.
5. S. BAUER and S. BAUER-GOGONEA, *IEEE Trans. Dielec. Elec. Insul.* **10** (2003) 883.
6. B. L. PHILLIPS, *J. Assoc. Comput. Mach.* **9** (1962) 84.
7. S. B. LANG, *Ferroelectrics* **118** (1991) 343.
8. P. BLOβ, M. STEFFEN, H. SCHAFER, Y. GUO MAO and G. M. SESSLER, *IEEE Trans. Dielec. Elec. Insul.* **3** (1996) 182.
9. P. BLOβ, M. STEFFEN, H. SCHAFER, G. EBERLE and W. EISENMENGER, *ibid.* **3** (1996) 417.
10. S. B. LANG, *ibid.* **5** (1998) 70.
11. T. SANDNER, G. SUCHANECK, R. KOEHLER, A. SUCHANECK and G. GERLACH, *Integr. Ferroelectr.* **46** (2002) 243.
12. WOLFRAM RESEARCH, Inc., Mathematica, Version 5.0, Champaign, IL, USA (2003).
13. C. ALQUIE, C. LABURTHE TOLRA, J. LEWINER and S. B. LANG, *IEEE Trans. Electr. Insul.* **27** (1992) 751.
14. A. MELLINGER, *Meas. Sci. Technol.* **15** (2004) 1347.
15. P. C. HANSEN and D. P. O$'$LEARY, *SIAM J. Sci. Comput.* **14** (1993) 1487.
16. H. AHLFELDT, J. WEBJORN and G. ARVIDSSON, *IEEE Photon. Tech. Lett.* **3** (1991) 638.
17. V. D. KUGEL and G. ROSENMAN, *App. Phys. Lett.* **23** (1993) 2902.
18. S. B. LANG, V. D. KUGEL and G. ROSENMAN, *Ferroelectrics* **157** (1994) 69.
19. T. PAWLOWSKI, S. B. LANG and R. FLEMING, in Proceedings of the 2004 Conference on Electrical Insulation and Dielectric Phenonema, Boulder, CO, USA (IEEE Service Center, Piscataway, NJ, USA, 2004) p. 93.
20. A. MELLINGER, R. SINGH, M. WEGENER, W. WIRGES, R. GERHARD-MULTHAUPT and S. B. LANG, *Appl. Phys. Lett.* **86** (2005) 82903.